VIS-IR study of brucite–clay–carbonate mixtures: Implications for Ceres surface composition

S. De Angelis [a,*], P. Manzari [a], M.C. De Sanctis [a], E. Ammannito [a,b], T. Di Iorio [a,c]

[a] *Istituto di Astrofisica e Planetologia Spaziali, INAF-IAPS, Via Fosso del Cavaliere, 100, 00133, Rome, Italy*
[b] *University of California Los Angeles, Earth Planetary and Space Sciences, Los Angeles, CA 90095, USA*
[c] *ENEA SSPT-PROTER-OAC, Centro Ricerche Casaccia, Via Anguillarese 301, 00123, Roma, Italy*

ARTICLE INFO

ABSTRACT

Carbonates and clay minerals are present in Solar System bodies such as Mars and asteroid (1) Ceres. Brucite has been proposed in the recent past to fit absorption features in spectra of Ceres. In this study Visible-Near Infrared reflectance spectroscopic measurements have been performed on brucite–carbonate–clay minerals mixtures, in the 0.2–5.1 µm spectral range. Different sets of three- and two-components mixtures have been prepared using these three fine powdered endmembers, by varying the relative proportions of carbonate, clay and brucite. Spectra have been acquired on the endmembers components separately and on the mixtures. Absorption features diagnostic of the carbonate, clay and brucite phases have been analyzed and band parameters (position, depth, area, width) determined. Several trends and correlations with mineral phase content in each mixture have been investigated, with the aim to determining how endmember components influence the mixture spectra and their minimum detectability threshold. Our results indicate that brucite is detectable in mineral mixtures with carbonates and clays, based on its main absorption features at 0.95, 2.45–2.47 and 3.05 µm. While the 0.95 and 3.05 µm features are only discernible for very high brucite contents in the mixtures, the ~2.45 µm band turns out to be highly diagnostic, also for very small amounts of brucite (of the order of 10 wt%). These experiments, together with DAWN observations of Ceres, substantially rule out the presence of great amounts of brucite globally distributed on the surface of Ceres.

1. Introduction

In the last years space missions to different Solar System objects have evidenced the presence of both carbonates and clay minerals of a wide range of types, on planetary bodies such as Mars (Ehlmann et al., 2008; Michalski and Niles, 2010; Ehlmann and Edwards, 2014; Fairen et al., 2010; Mustard et al., 2008; Murchie et al., 2009; Vaniman et al., 2014). Carbonate–clay mixtures (Rivkin et al. 2006; Carry et al. 2008), and carbonate–brucite mixtures (Milliken and Rivkin, 2009a,b; Zolotov, 2009) have been so far proposed in order to explain the surface composition of the Asteroid 1-Ceres, as derived by ground-based telescopic reflectance spectra in the near-infrared range. In particular brucite $(Mg(OH)_2)$ has been invoked in order to explain the absorption feature at 3.05 µm observed in Ceres telescopic reflectance spectra (Milliken and Rivkin, 2009a,b), although the same feature has been tentatively explained in the past also with the presence of water ice frost (Lebofsky et al., 1981), ammonium-bearing minerals

such as NH_4-saponite (King et al., 1992), ion-irradiated organic material (Vernazza et al., 2005), hydrated iron-bearing phyllosilicates (Rivkin et al., 2006). New data from VIR spectrometer (De Sanctis et al., 2011) on-board DAWN mission (Russell et al., 2004) provided further insights and constraints about the Ceres surface composition confirming the presence of phyllosilicates, ammoniated phyllosilicates, carbonates and a dark component, likely magnetite (De Sanctis et al., 2015).

Brucite is not very common on Earth and in the Solar System as native mineral phase; it mainly occurs as aqueous alteration product of periclase (MgO) in presence of Mg-carbonates (Frost and Kloprogge, 1999) or alteration of Mg-rich peridotites. For example the hydration of Mg-rich olivine is given by the reaction of production of serpentine and brucite (Frost and Beard, 2007):

$$2\ Mg_2SiO_4 + 3\ H_2O = Mg_3Si_2O_5(OH)_4 + Mg(OH)_2$$

The brucite layered structure consists of two sheets of hydroxyls containing a sheet of Mg cations between them; each Mg ion is in the center of an octahedron of OH anions. Brucite sheets also typically constitute the intimate structure of phyllosilicates containing divalent cations such as Mg^{2+} or Fe^{2+}.

* Corresponding author.
  E-mail address: simone.deangelis@iaps.inaf.it (S. De Angelis).

Table 1

Chemical compositions of the endmembers used for the mixtures.

Component	Constituent	wt%
Brucite	Brucite [$Mg(OH)_2$]	90
	Lizardite [$Mg_3Si_2O_5(OH)_4$]	2
	Rodolicoite [$Fe^{3+}PO_4$]	1
	B-Mullite [$Al_{4+2x}Si_{2-2x}O_{10-x}$]	1
	Magnesite [$MgCO_3$]	1
	Quartz [SiO_2]	1
	Dolomite [$CaMg(CO_3)_2$]	3
Carbonate (GPR18)	Dolomite	92
	Ankerite [$Ca(Mg,Fe^{2+},Mn)(CO_3)_2$]	8
Clay (MLA4)	Illite [$(K,H_3O)\bullet(Al,Mg,Fe)_2]\bullet[(Si,Al)_4O_{10}]\bullet[(OH)_2,(H_2O)]$	37.6
	Quartz	47.5
	Calcite [$CaCO_3$]	12.9
	Magnetite [Fe_3O_4]	1
	Birnessite [$(Na_{0.3}Ca_{0.1}K_{0.1})(Mn^{4+},Mn^{3+})_2O_4*1.5H_2O$]	1

For what concerns Ca-carbonates, on Earth the primary mechanism of formation is given by sedimentation of pelagic skeletals organisms in deep-water (calcite) or shallow-water (aragonite and Mg-rich calcite) marine environments, mostly at low to middle latitudes (Morse, 2003). Another mechanism is evaporation in saline lakes (Jones and Deocampo, 2003). However if carbonates occur on other Solar System bodies, such as asteroids, different formation mechanisms have to be invoked. Calcium (but also Mg-, Mn-, Fe-) carbonates and clay minerals found in CI and CM chondrite meteorites (Fredriksson and Kerridge, 1988; Endress and Bischoff, 1996; Tonui et al., 2014) are supposed to have been formed by low-temperature aqueous alteration of primary mafic minerals on meteorites parent bodies regoliths (Fredriksson and Kerridge, 1988; Johnson and Prinz, 1992; Endress and Bischoff, 1996). The process of condensation of carbonates directly in the solar Nebula is instead generally ruled out because of the observed high degree of elemental fractionation (Fredriksson and Kerridge, 1988), although they have been more recently found in interstellar medium (Toppani et al., 2005). Aqueous alteration of olivines can also produce carbonates (D'Amico et al., 1989; Staudigel, 2003). The heat source necessary for circulation of fluids within asteroidal regoliths and subsequent aqueous alteration is justified as induced by impact processes or radiogenic heating (Endress and Bischoff, 1996). Chemical variations among the different cation concentrations (Fe^{2+}, Mn^{2+}, Ca^{2+}, Mg^{2+}) imply different conditions and regimes of circulating fluids (Johnson and Prinz, 1992). Other formation mechanisms are for example carbonation reactions, in which carbonate is produced by interaction of calcium hydroxide with CO_2, or Mg-carbonate is produced by reaction of brucite with CO_2 (Garenne et al., 2013). More generally Mg- or Fe-rich olivines and Ca-rich pyroxenes can react with CO_2 to form magnesite, siderite or calcite, respectively (O'Connor et al., 2005).

In this work we perform spectroscopic analyses in the VIS-IR on brucite–carbonate–clay mineral particulate mixtures, which have relevance for Ceres; two- and three-component mixtures have been investigated varying each of the components in different proportions. Spectral parameters of endmembers and all mixtures are retrieved and analyzed in order to derive detectability thresholds of each component, and to fix constraints for Ceres' surface composition.

2. Experiment

2.1. Experimental setup

Spectroscopic measurements have been performed with the Spectral Imaging (SPIM) facility in use at the laboratory of IAPS-

INAF. The facility is described in detail in Coradini et al. (2011) and De Angelis et al. (2015). It is an imaging spectrometer spare of the VIR instrument onboard the Dawn mission to Vesta and Ceres (De Sanctis et al., 2010). It operates in the visible and infrared spectral range 0.2–5.1 μm, using a CCD detector in the VIS channel (0.2–1.0 μm) and a HgCdTe detector in the IR channel (1.0–5.1 μm). It is characterized by high spatial resolution of 38 μm/pixel and spectral resolution of 2 nm in the VIS and 12 nm in the IR channels, respectively. The radiation sources are a QTH lamp in the VIS and an IR emitter that is used in 2.5–5.1 μm range.

The light scattered by the observed target is conveyed through an optical system constituted by both flat and parabolic off-axis mirrors to an Offner spectrometer, whose entrance slit is $9 \times 0.038 \, mm^2$ in size. The diffraction grating allows then to analyze the spectral components of light on the VIS and IR focal planes. An image strip of $9 \times 0.038 \, mm^2$ is acquired on the target with a single acquisition: a motorized three-axes sampleholder allows to acquire a two-dimensional scan of the target, thus permitting the construction of a data-cube, having the spectral information along the third dimension. All samples have been measured under ambient P-T conditions.

2.2. Analyzed samples

Three different end-member samples have been chosen in order to simulate mixtures: (i) a carbonate sample, micritic limestone from Italian Apennines (GPR18; Ernici Mountains); (ii) a clay sample, from Italian Apennines (ML-A-4; Lepini Mountains); (iii) brucite, that is magnesium hydroxide, $Mg(OH)_2$ (commercial, Garrison Minerals). The carbonate and clay were ground and dry sieved, starting from fragments, at a grain size $d<20 \, \mu m$; the brucite was provided by the company in fine powder form with grain size $d>10 \, \mu m$. Four sets of mixtures have been prepared by manually mixing these end-members in different weight proportions: (i) the carbonate proportion is kept fixed at 10 wt%, while varying the amounts of clay and brucite; (ii) the carbonate proportion is kept fixed at 40 wt%, while the amounts of clay and brucite are varied; (iii) the carbonate proportion is kept constant at 70 wt% and the amounts of clay and brucite are then varied; (iv) the fourth set consists of two-components mixtures with no carbonate content. For all mixtures it has been assumed an amount of 10 g as the 100 wt% reference.

X-Ray Diffraction analyses have been performed at the University of Bari on all endmember samples, brucite, GPR18 and MLA4, although the chemical composition of brucite was also provided by the seller company. XRD analyses have been performed with a Diffrattometer Empyrean, Panalytical, at 40 kV/40 mA and CuKα
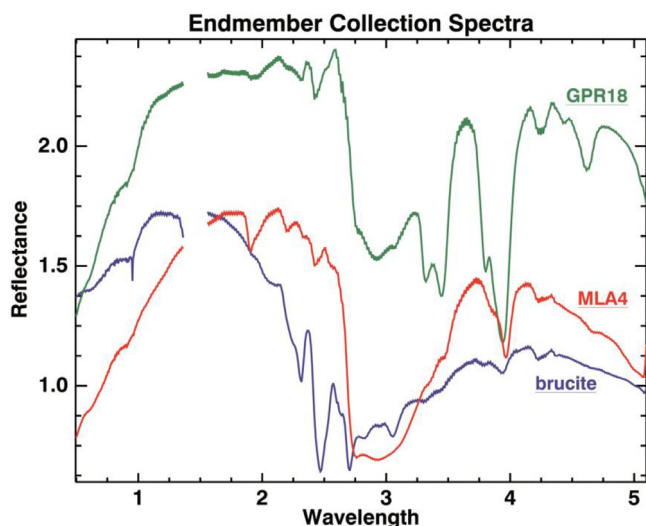
Fig. 1. Spectra of the three end-members used to prepare the mixtures. The curves are shifted in reflectance for clarity.

radiation. The compositions are listed in Table 1. For what concerns the clay-mineral with illitic composition, we have to note that the amounts of quartz and magnetite do not add absorption features; they only have an impact on the reflectance level of the sample. Moreover their contributes likely compensate each other, because quartz rises the reflectance level while a few percent of magnetite lowers the reflectance considerably. The 12 wt% calcite add carbonate bands visible in the spectra (see Sections 4.2 and 4.3).

3. Results

3.1. Reflectance spectra: end-members

The spectra of end-members are shown in Fig. 1. The spectrum of the dolomitic limestone sample (GPR18) is characterized by a weak H_2O absorption near 2 μm, by a broad H_2O feature at 3 μm, and by CO_3 absorption bands near 3.4, 3.9 (very deep) and 4.6 μm. In the case of GPR18 sample, H_2O-related features are likely due to some adsorbed water in ambient conditions. The illitic clay spectrum shows absorption features near 1.9 μm (H_2O), two bands at 2.2 and 2.45 μm (Al–OH), a very broad water absorption band at 3 μm, and a CO_3 feature at 3.9 μm. Other weak features attributable to some minor CO_3 content appear at 3.4 μm (as a shoulder) and 4.6 μm. The spectrum of brucite (Fig. 2) is characterized by the very narrow OH absorption appearing at 1 μm and by Mg–OH absorption features occurring at 2.1 and 2.3 μm. The 2.45–2.47 μm feature can also be due to Mg–OH, as measured by Beck et al. (2015) on brucite spectra. The band near 3 μm is attributable to water; a feature at 2.75 μm is due to OH and the other one at approximately 3.05 μm is related to combination of OH and lattice bands in brucite (Beck et al. 2015). A few carbonate content in this sample is seen by weak absorptions at 3.4 and 3.9 μm: magnesite (Mg-carbonate) is indeed readily produced after reaction of brucite with CO_2. Carbon dioxide in the room could
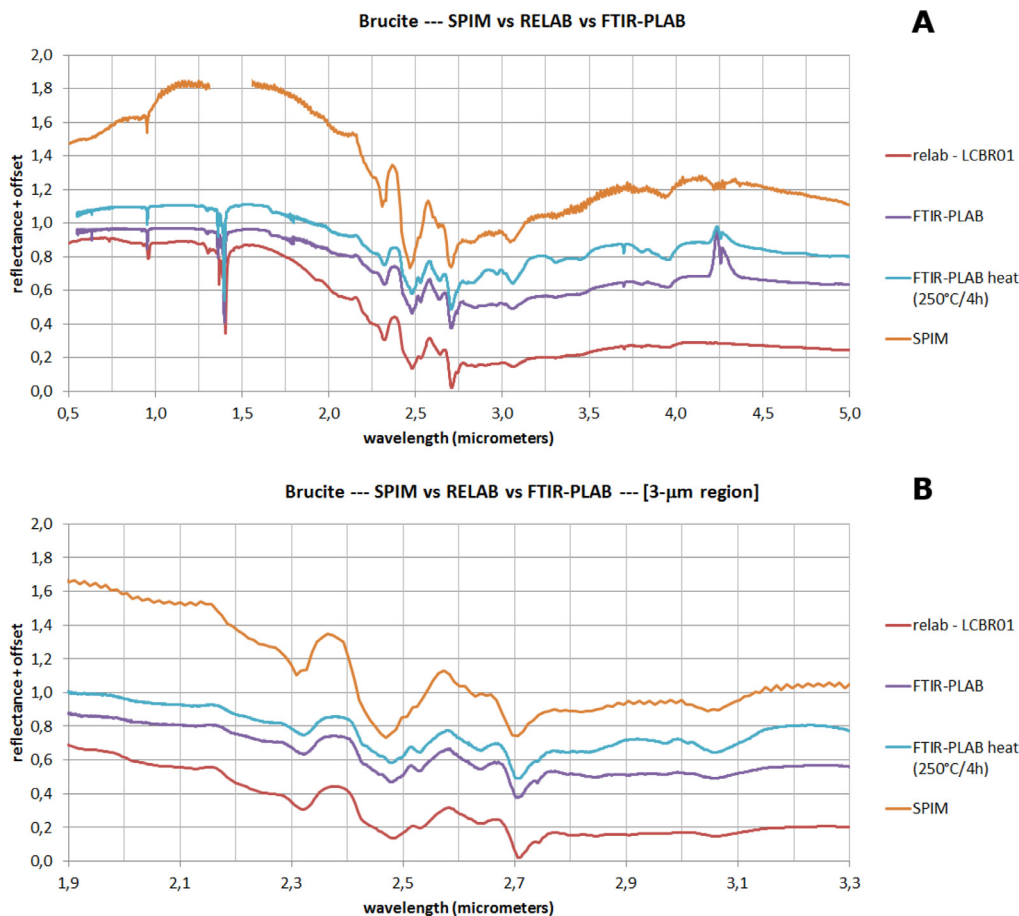

Fig. 2. A comparison of brucite spectra between SPIM measurements (blue curve) and RELAB spectral library (green and red, two different grain sizes). B: zoom on the 3 μm spectral region. Data at 1.4 μm not shown for instrumental artifact. The emission peak at 4.25 μm is due to CO_2 in the laboratory. (For interpretation of the references to color in this figure legend, the reader is referred to the web version of this article).
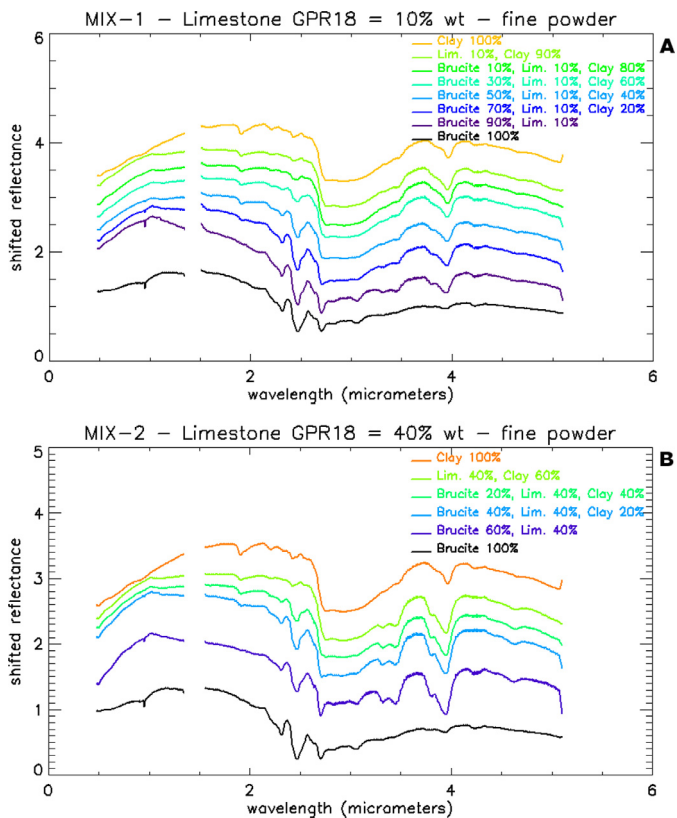
Fig. 3. A spectra of the mixture Mix-1, with carbonate (GPR18) content of 10 wt%. B: spectra of mixture Mix-2, with carbonate content of 40 wt%. The spectra are shifted in reflectance for clarity. Instrumental artifacts near 1.4 are not shown. (For interpretation of the references to color in this figure, the reader is referred to the web version of this article).

Fig. 4. A spectra of Mix-3, with carbonate content equal to 70 wt%. B: spectra of Mix-4, containing no carbonate. The spectra are shifted in reflectance for clarity. Instrumental artifacts near 1.4 μm are not shown.

Fig. 5. Spectra of 2-components mixtures. A: brucite + carbonate (GPR18) mixtures. B: clay (MLA4) + carbonate (GPR18) mixtures. The spectra are shifted in reflectance for clarity. Instrumental artifacts near 1.4 μm are not shown.

also be responsible for the small feature at 4.2 μm appearing in all spectra, although matching with a similar feature in carbonate spectra. Data at 1.4 μm are not shown due to an instrumental artifact.

3.2. Reflectance spectra: mixtures

3.2.1. Mix-1: carbonate content 10 wt%

The first set of mixtures is defined by a carbonate content equal to 10 wt%. The spectra are in Fig. 3A. The end-member spectra of clay and brucite are also plotted. The spectral profiles show several gradual variations as the relative amounts of brucite and clay vary. At high brucite content the narrow OH absorption at 1 μm remains visible; the 2.45 μm feature seems to get more deeper as the brucite content increases, confirming that this band is real. The increasing brucite content also produces a more negative blue slope. The 2.7 μm OH feature in brucite is discernible in the mixtures containing very small amounts of MLA4-clay (<20 wt%), while it persists in mixtures with high GPR18-carbonate content (<70 wt%). The 3.05 μm band is visible only in the mixture with high content of brucite and tends to disappear in the large 3 μm feature of the clays for lower brucite abundance.

3.2.2. Mix-2: carbonate content 40 wt%

In the ternary mixtures with a fixed carbonate content (40 wt%, spectra in Fig. 3B), the OH 1 μm band is still visible for the mixtures with brucite content higher than 90%. The 2.1, 2.3 and 2.45 μm Mg–OH brucite bands tend to increase in strength at increasing brucite content, while the 1.9 μm H₂O band tends to disappear. All the spectra of the mixtures show carbonate bands at 3.4 and 3.9 μm, while the 4.6 μm feature is very weak.
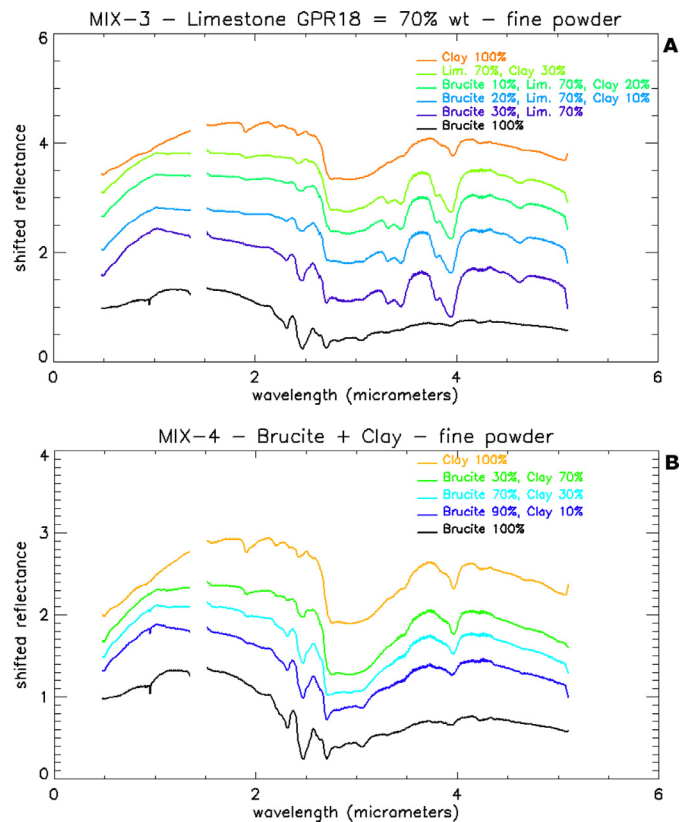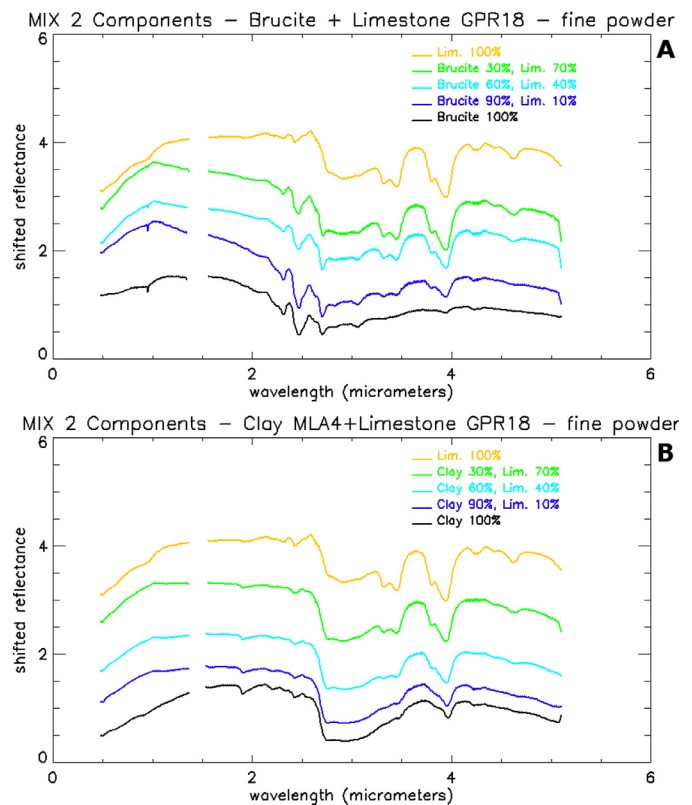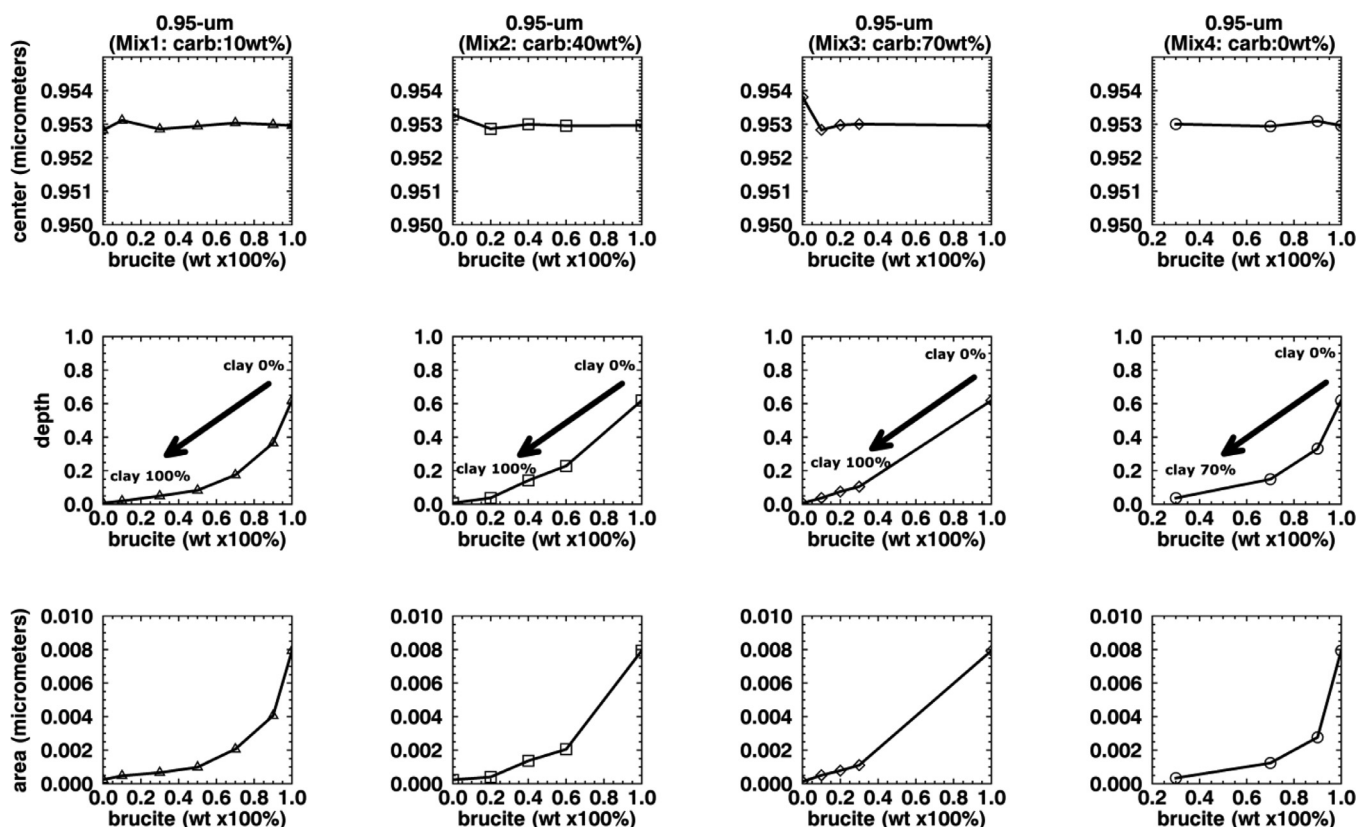
Fig. 6. Band parameters (center, depth, area) of the 0.95-micron OH-band of brucite. Parameters are plotted as functions of brucite and clay content (wt%), for each fixed value of carbonate in the mixture.

3.2.3. Mix-3: carbonate content 70 wt%

The third set of three-components mixtures (spectra in Fig. 4A) has an even higher carbonate content (70 wt%). The brucite OH narrow feature at 1 μm is no longer visible in the spectra of mixtures. The 2.2 μm Al–OH band in clay disappears and the 2.3 μm Mg–OH band of brucite appears, as the content of the latter increases; The 3.05 μm band typical of brucite is not recognizable in the spectra of the 70 wt% mixtures, while the 2.45 μm remains visible even with only 10% of brucite in the mixture. The spectra are dominated by intense bands of carbonate at 3.4, 3.9 μm, superimposed on the broad H_2O band near 3 μm.

3.2.4. Mix-4: carbonate content 0 wt%

The last set consists of two-component mixtures, containing no carbonate (Fig. 4B). The 1.9 μm H_2O band of clay is still visible for clay content down to 30 wt%; for brucite content of 70 wt% and higher the 2.3 μm Mg–OH band is clearly discernible. Some amount of carbonate material within clay is evidenced by the feature at 3.9 μm. Also in this case, the 3.05 μm band typical of brucite is broadly recognizable in the spectra of the mixtures with high brucite content (>70 wt%), while the 2.45 μm remains visible even with only 30% of brucite in the mixture.

The other two sets of 2-components mixtures, extracted from all the ones measured, are show for clarity in Fig. 5. Brucite–carbonate (GPR18) mixtures are shown in Fig. 5A. In the absence of clay, the diagnostic features of brucite in the 2.7–3 μm region are still visible for a minimum brucite content of 30 wt%. In MLA4-GPR18 mixtures (Fig. 5B) the carbonate features in the 3.4–4 μm region are clearly discernible for a minimum limestone content of 40 wt%.

4. Analysis and trends

Spectral band parameters have been computed for several diagnostic absorption features for the three endmembers and for the four sets of mixtures. All spectra have been scaled at 1 in reflectance, prior to perform any further data analysis, thus neglecting any albedo information. A smoothing of order 2 has been applied in the 1–5 μm range, in order to reduce odd-even noise. Subsequently, for each analyzed band the background continuum has been removed dividing the reflectance by the straight line joining the band edges, at each wavelength. After continuum removal, the parameters position, depth, area and width have been computed. The band position (center) has been retrieved selecting a region near the minimum, and then computing the center with a 2nd order polynomial fit after having resampled with a denser number of points. The depth has been calculated as $B_D = 1 - R_B/R_C$ (Clark and Roush, 1984), where R_B is the reflectance at the band center and R_C is the reflectance at the continuum, at band center. The area has been computed as the integral of the band between the edges. The width has been calculated at half of the band depth.

4.1. Brucite

Concerning the absorption bands related to brucite, the features at 0.95 μm (O–H), 2.1 μm, 2.3 μm and 2.45 μm (MgOH), 2.7 μm (O–H) and 3.05 μm (O–H) have been analyzed as a function of brucite wt% content in the mixtures. The O–H brucite band in the 1.4 μm-region has not been considered because an instrumental artifact completely overlaps this feature in the same region.

The narrow O–H feature at 0.95 μm tends to disappear, decreasing in depth, area and width as the clay content becomes greater (Fig. 6). In the mixture set-1 (carbonate 10 wt%) this
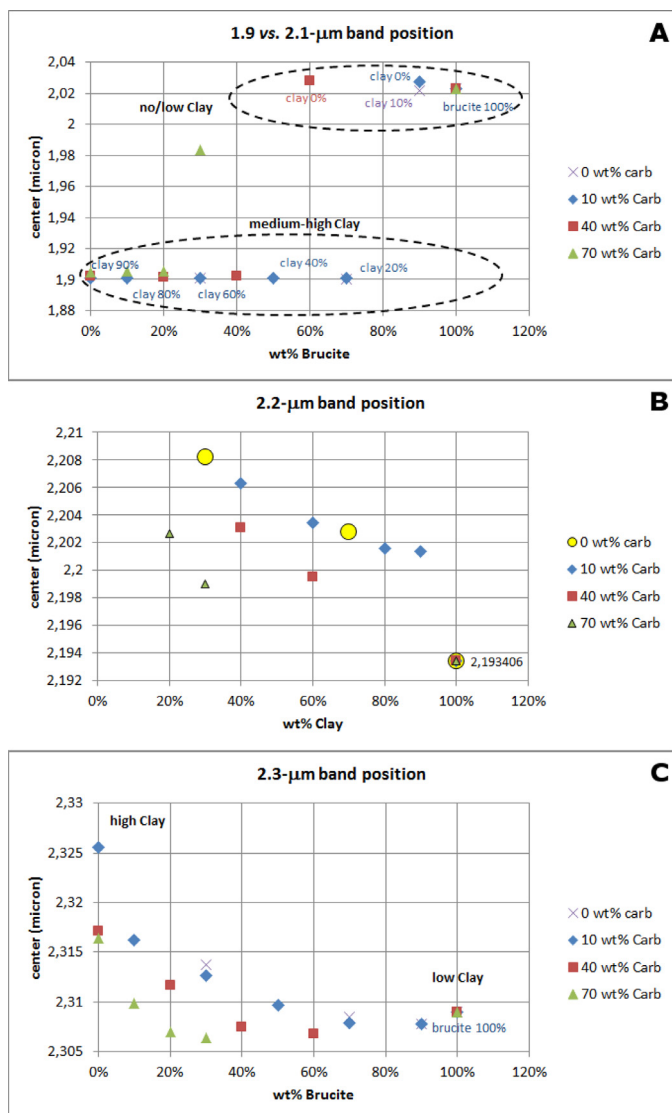
Fig. 7. A center of the 2.1 μm feature of brucite; this band rapidly disappears, while the clay 1.9 μm feature appears, as the clay content increases. B: center of the 2.2 μm feature of clay. C: center of the 2.3 μm feature of brucite. This band disappears while the clay 2.35 μm feature appears as the clay content increases.

diagnostic feature is clearly discernible for brucite content in the range 100–50 wt%. The band depth decreases of a factor 50% when the brucite content decreases from 100 to 80 wt%; the band area decrease of a factor 50% when the brucite decreases from 100 to 90 wt%. In the mixture set-2 (carbonate 40 wt%) this feature is still recognizable for a minimum brucite content of 60 wt%. In the mixture set-3 (carbonate 70 wt%) this narrow diagnostic feature is no longer identifiable. Finally in the set-4 of mixtures (two components, no carbonate) this band is recognizable for a brucite content in the range 100–70 wt%. The band center doesn't show significant shift in wavelengths in the different mixtures.

The brucite Mg–OH feature near 2.1 μm rapidly disappears, while the feature near 1.9 μm appears, at high values of clay content in the mixture (Fig. 7). The Mg–OH feature near 2.3 μm tends to decrease both in depth and area, as the brucite proportion becomes smaller, and the clay content increases (Figs. 7 and 8). At the same time this feature gradually disappears, as the clay content increases: a band gradually appears centered near 2.2 μm for clay content in the range 60–100 wt%, and could be related to Al-OH in the clay phase (see also Clark et al., 1990, for bands assignment).

A similar analysis has been carried out also on the feature near 2.45 μm that, although occurs near the instrumental artifact, shows a correlation with the brucite content in the mixtures. Looking at the plot in Fig. 2 indeed the measured brucite spectral profile in the 2.1–3.3 μm region appears very similar to library spectra (RELAB database). The retrieved trends are shown in Fig. 9. Both band depth and area are characterized by a general decrease as the brucite content increases. The band position again shifts towards shorter wavelengths with increasing clay content.

The brucite feature at 2.7 μm has also been studied. Band parameters have been determined in two ways, both considering only the relative peak-minimum at 2.7 μm (Fig. 10), and considering the whole 3 μm feature (Fig. 11). The 2.7 μm feature maintains its individuality for brucite content in mixtures of at least > 50 wt%. For brucite < 40–50 wt% the minimum at 2.7 μm is no longer discernible (Fig. 10). The addition of small amounts of clay (<20 wt%) in the mixtures causes the feature rapidly to disappear (band depth and area increase), because of the presence of water 3 μm feature (Figs. 10 and 11).

The absorption band at 3.05 μm is clearly discernible in 3-components mixtures containing an amount of brucite of at least > 60–70 wt% or more (Figs. 3,4 and 12); for smaller amounts of brucite, the presence of this feature results in a weak distortion of the 3.0 μm water band. When only carbonate is added in the mixture with brucite, the 3.05 μm feature shifts towards longer wavelengths, because of increasing and broadening of the carbonate 3.4 μm band; at the same time the computed depth decreases. When only clay instead is added in the mixture with brucite, the increasing and broadening of 3 μm clay water band causes the 3.05 μm feature to shift towards longer wavelengths and to rapidly lose its distinctness, below a threshold brucite content of about 70 wt% (Fig. 12). In both cases adding carbonate or clay to brucite (2-component mixture), the increasing of 3.4 μm or 3.0 μm absorption bands, respectively, essentially causes a modification of the continuum line and of the whole band.

4.2. Clay (ML-A-4)

Concerning the clay component, the H$_2$O band near 1.9 μm has been evaluated (Fig. 13). The water absorption feature maintains its individuality for clay amounts from 100% down to about 20 wt%. For lesser amount of clay in the mixture this band disappears and a weak feature near 2.1 μm due to brucite appears. For high brucite contents, both depth and area decrease monotonically, while the width shows a more irregular behavior. The 1.9 μm band is also influenced by the presence of carbonate in the mixture, which also shows an absorption in the same region (see next section).

4.3. Carbonate (GPR18)

The H$_2$O 1.9 μm feature in mixtures is due to the presence of both clay and carbonate. In Fig. 14 it is shown how the carbonate content influences the band area; the areas corresponding to clay contents of 30 wt% and 60 wt% in the mixtures containing no carbonate (MIX-4, Fig. 4B) assume values of about 0.02 and 0.04 μm, respectively. The band areas increase linearly after the addiction of some amount of carbonate in the mixtures (for carbonate contents equal to 10, 40 and 70 wt%).

Then for each analyzed set of mixtures, corresponding to a fixed value of carbonate wt% content, the average band depth for the carbonate features at 3.4, 3.9 and 4.6 μm has been computed. Band depth and area values have been averaged over the different mixtures (with variable clay/brucite proportions) corresponding to each carbonate content, and then plotted vs. carbonate content (Fig. 15A and B). The depth of each band increases as the carbonate amount in the mixture increases.
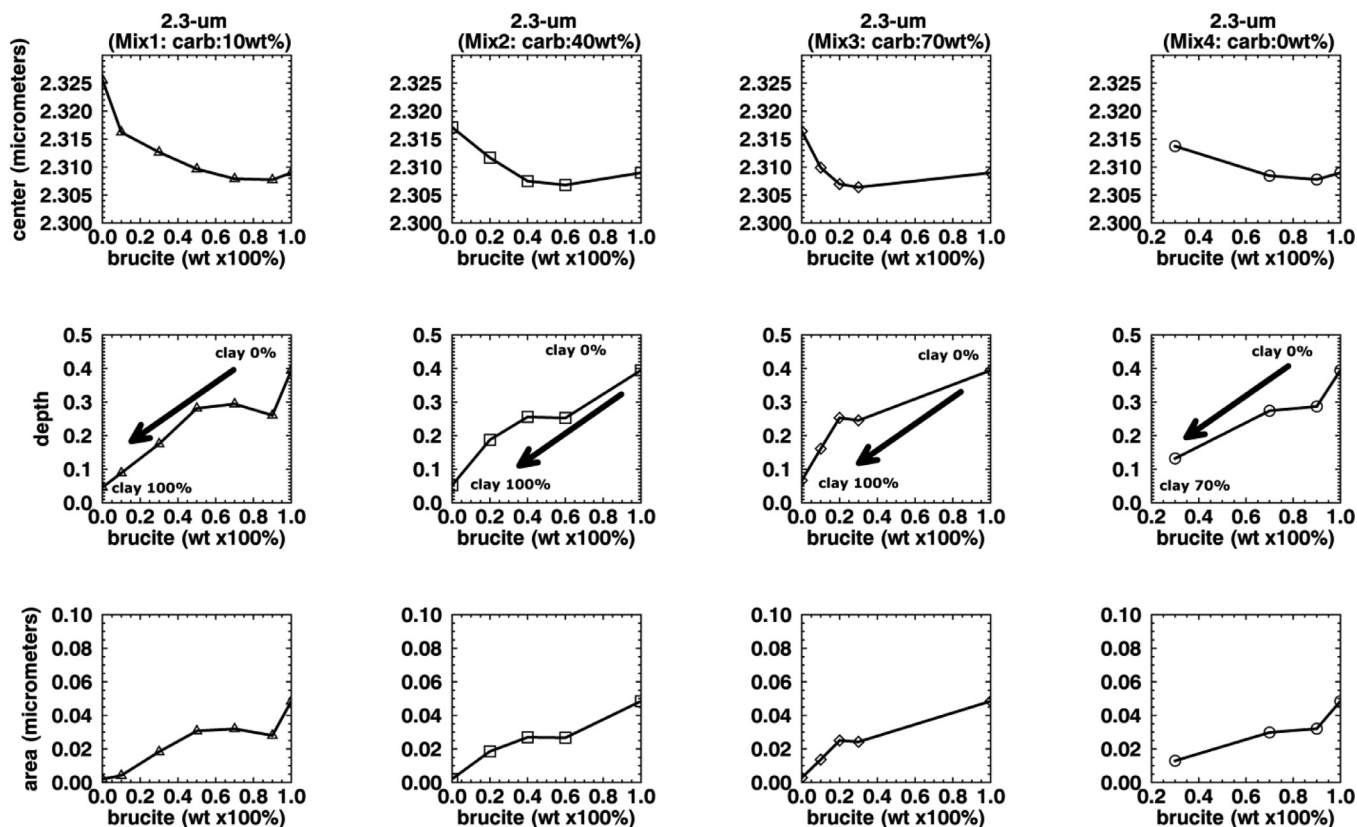
Fig. 8. Band parameters (center, depth, area) of the 2.3-micron Mg–OH band of brucite. Parameters are plotted as functions of brucite and clay content (wt%), for each fixed value of carbonate in the mixture.
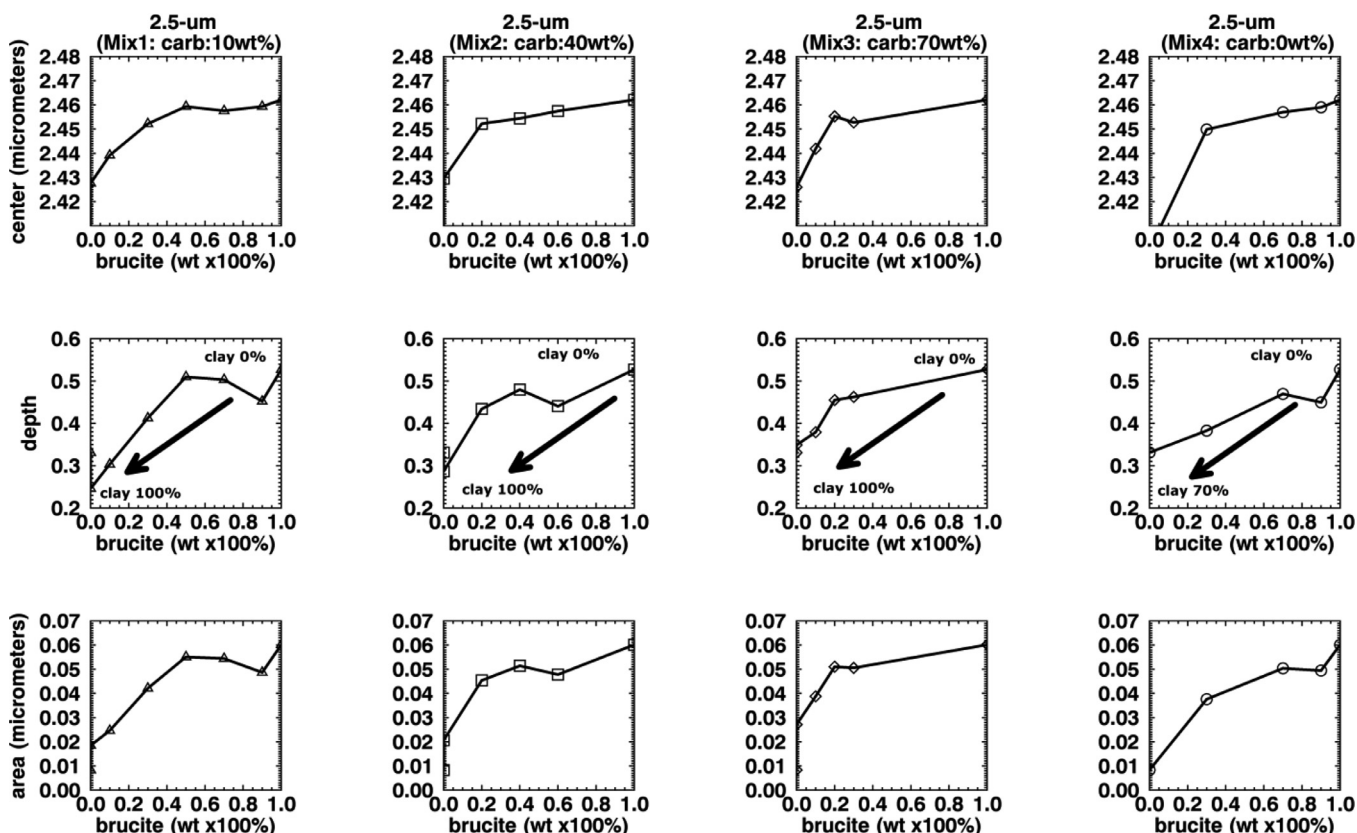

Fig. 9. Band parameters (center, depth, area) of the 2.45-micron Mg–OH band of brucite. Parameters are plotted as functions of brucite and clay content (wt%), for each fixed value of carbonate in the mixture.
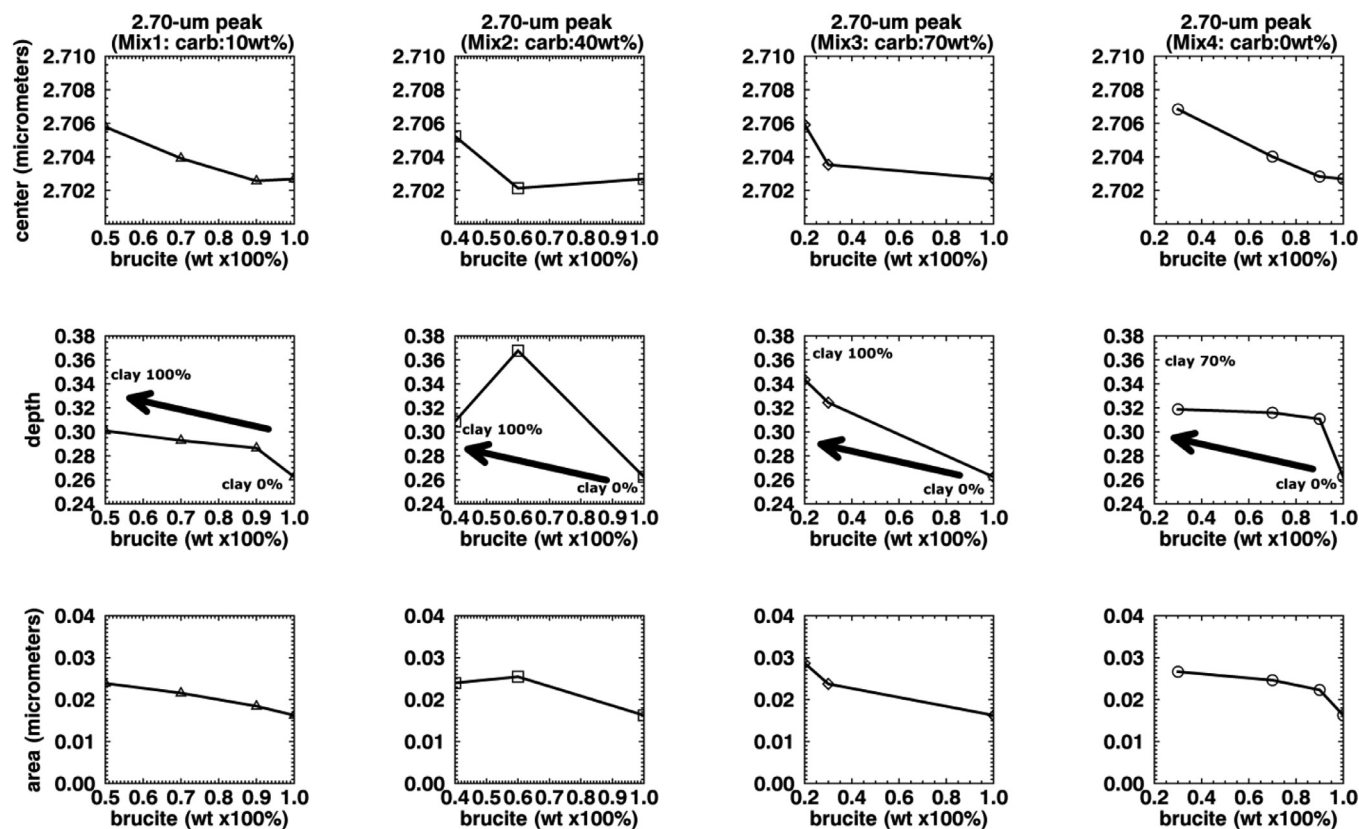
Fig. 10. Band parameters (center, depth, area) of the 2.70-micron OH band of brucite (peak). Parameters are plotted as functions of brucite and clay content (wt%), for each fixed value of carbonate in the mixture.
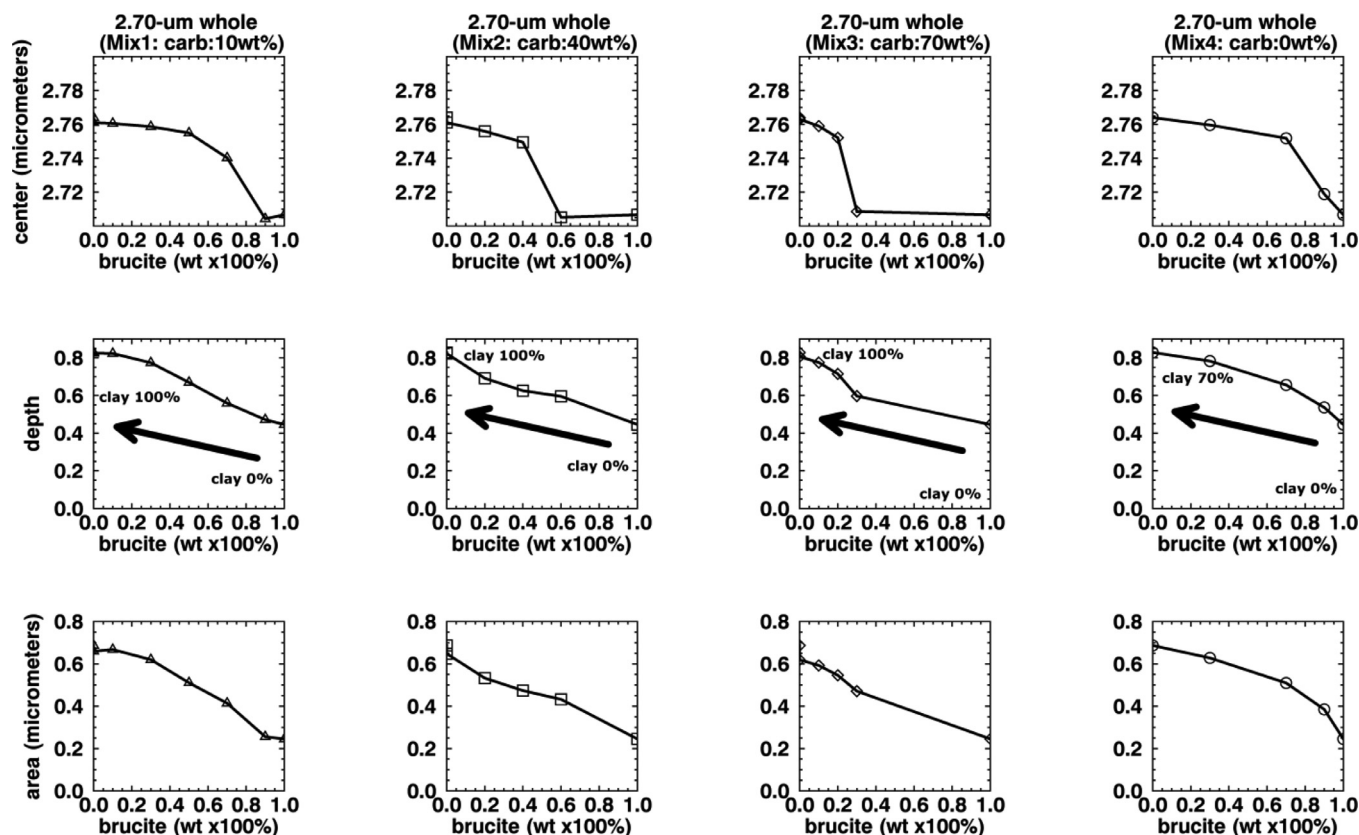

Fig. 11. Band parameters (center, depth, area) of the 2.70-micron OH band of brucite (whole H_2O band). Parameters are plotted as functions of brucite and clay content (wt%), for each fixed value of carbonate in the mixture.
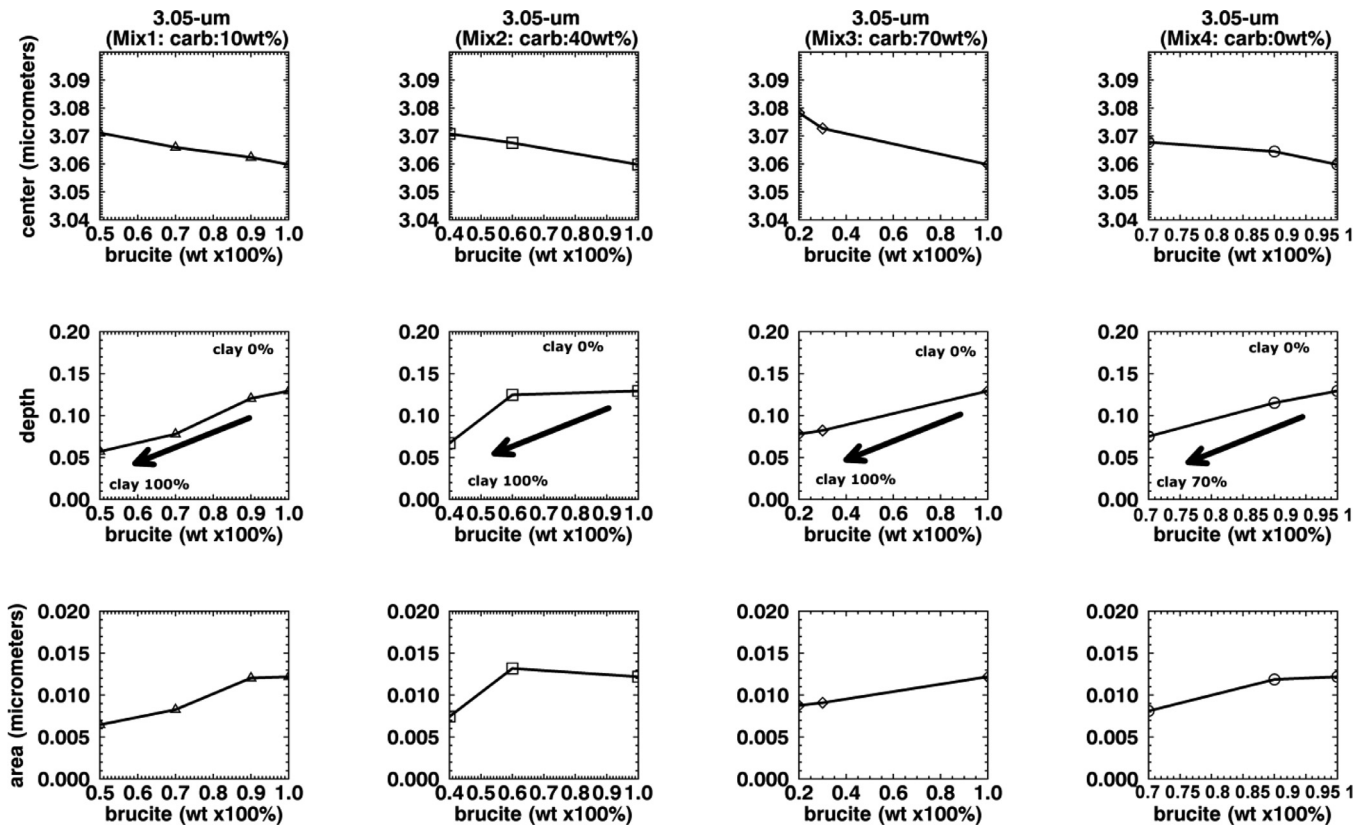
Fig. 12. Band parameters (center, depth, area) of the 3.05-micron feature of brucite. Parameters are plotted as functions of brucite and clay content (wt%), for each fixed value of carbonate in the mixture.
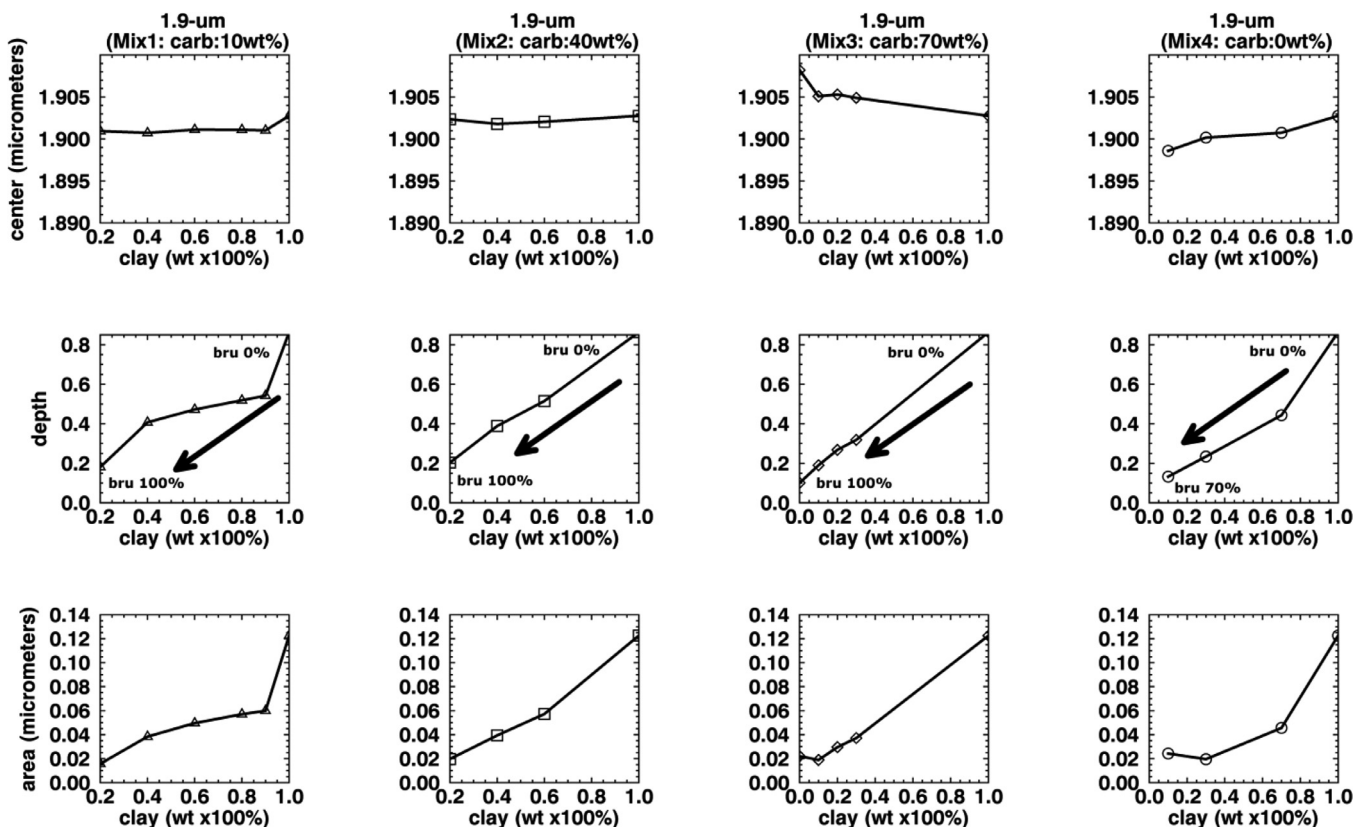

Fig. 13. Band parameters (center, depth, area) of the 1.9-micron H$_2$O-band of clay (ML-A-4). Parameters are plotted as functions of clay and brucite content (wt%), for each fixed value of carbonate in the mixture.
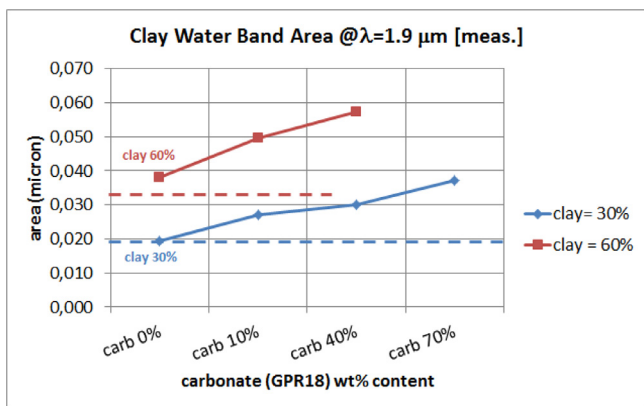
Fig. 14. Band area of 1.9 µm water absorption feature, due to clay. The addition of carbonate in the brucite–clay mixture causes the 1.9 µm band area to increase linearly with the carbonate content.

The 3.9 µm absorption feature also occurs in clay and brucite. In the case of clay this indicates a small amount of carbonate content (calcite; see Table 1 and Section 2.2), while in the case of brucite it likely implies some carbonation reaction of $Mg(OH)_2$ with ambient CO_2. In Fig. 16A the 3.9 µm feature spectral profiles for the three endmembers are shown, after continuum removal: they are centered at 3.94 (brucite), 3.94 (carbonate GPR18) and 3.96 µm (clay MLA4) (see Table 2). The band depths are in the ratios D_{BRU}/D_{CARB} = 0.17 and D_{CLA}/D_{CARB} = 0.65, while the band areas are in the ratios A_{BRU}/A_{CARB} = 0.10 and A_{CLA}/A_{CARB} = 0.39, that is the band area at 3.9 µm in the clay MLA4 endmember is approximately 40% of the band area at 3.9 µm in the limestone GPR18 endmember. The band area trends at 3.4 and 3.9 µm (Fig. 15B) indicate that area values are not decreased by a factor of 10 when passing from 100 wt% GPR18 (endmember) to 10 wt% (Mix-1), but by a factor 5 and 2.5, respectively, indicating the contribution of clay and brucite.

In Fig. 16B the 4.6 µm absorption feature spectral profiles are reported for the two endmembers carbonate (GPR18) and clay (MLA4). The brucite endmember did not show any appreciable absorption feature at this wavelength. The band depth and area ratios are D_{CLA}/D_{CARB} = 0.12 (consistent with 12 wt% content of calcite within MLA4) and A_{CLA}/A_{CARB} = 0.08, respectively. The band is centered at 4.62 µm in the GPR18 sample and at 4.66 µm in the clay MLA4 sample (Table 2), suggesting some difference in the carbonate composition (indeed, dolomite vs. calcite). The clay/carbonate area ratio A_{CLA}/A_{CARB} = 0.08 at 4.6 µm indicates that this absorption feature is nearly negligible in the clay MLA4 sample, with respect to the feature appearing in the carbonate GPR18 sample. Thus it is diagnostic and can be used to trace the content of GPR18-carbonate within each mixture. The linear relation between 4.6 µm

Table 2

End-members weight proportions used to construct the four sets of mixtures. The Mix-1, Mix-2 and Mix-3 are three-component mixtures, while the Mix-4 is a two-component mixture, containing no carbonate.

Mix-1	Carbonate (GPR18) = 10 wt%		
	Brucite (%)	Carbonate (%)	Clay (%)
Cer1a	90	10	0
Cer1b	70	10	20
Cer1c	50	10	40
Cer1d	30	10	60
Cer1e	10	10	80
Cer1f	0	10	90
Mix-2	Carbonate (GPR18) = 40 wt%		
	Brucite (%)	Carbonate(%)	Clay (%)
Cer2a	60	40	0
Cer2b	40	40	20
Cer2c	20	40	40
Cer2d	0	40	60
Mix-3	Carbonate (GPR18) = 70 wt%		
	Brucite (%)	Carbonate (%)	Clay (%)
Cer3a	30	70	0
Cer3b	20	70	10
Cer3c	10	70	20
Cer3d	0	70	30
Mix-4	Carbonate (GPR18) = 0 wt%		
	Brucite (%)		Clay (%)
Cer4a	90		10
Cer4b	70		30
Cer4d	30		70

Table 3

Band parameters of absorption features at 3.9 and 4.6 µm in the analyzed endmember samples.

3.9 µm band	Depth	Area (µm)	Position (µm)
Carbonate (GPR18–dolomite)	0.83	0.24	3.94
Clay (MLA4 – calcite)	0.54	0.09	3.96
Brucite (dolomite)	0.14	0.02	3.94
4.6 µm band	Depth	Area (µm)	Position (µm)
Carbonate (GPR18–dolomite)	0.42	0.059	4.62
Clay (MLA4 – calcite)	0.049	0.005	4.66

band parameters and GPR18-carbonate content in the mixtures is reported in Table 3. The carbonate endmember (GPR18 = 100 wt%) shows indeed a 4.6 µm band area equal to 0.059 (Table 2). The average band area at 4.6 µm computed for the set of mixtures MIX-1 (GPR18 = 10 wt%) is instead about 0.007, that is lower than a factor 10 (Supplementary material, Table 32).
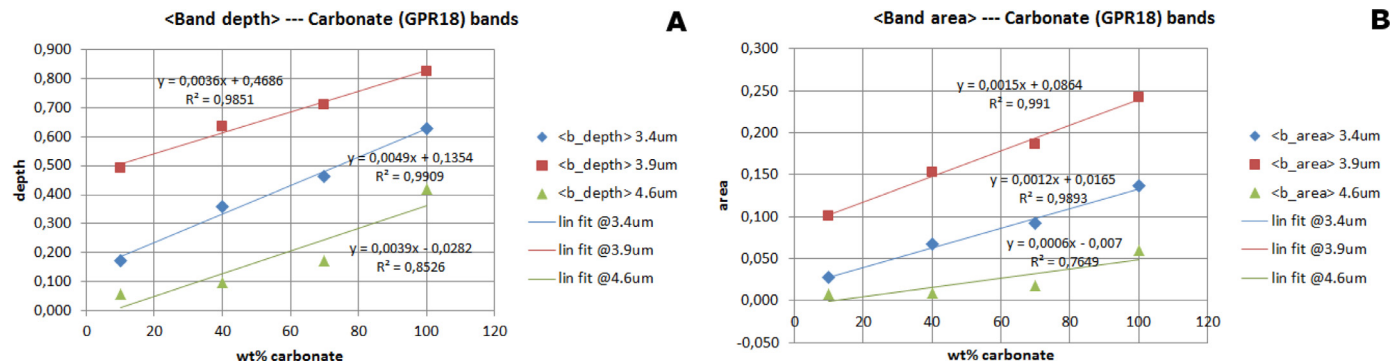

Fig. 15. Average band depth (A) and area (B) of carbonate absorption features centered at 3.4, 3.9 and 4.6 µm, vs. carbonate wt% content (GPR18) in the mixture set.
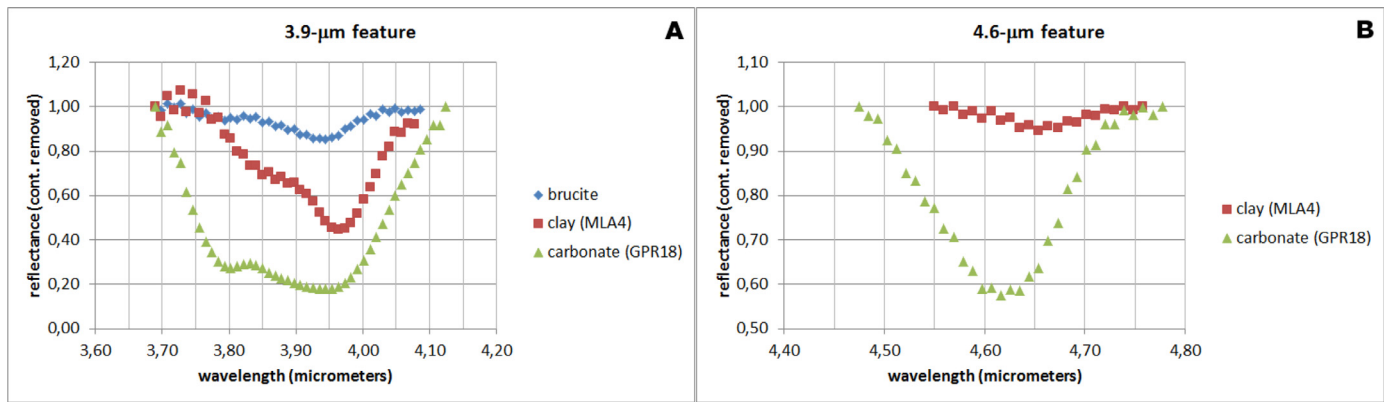
Fig. 16. Absorption features at 3.9 µm (A) and 4.6 µm (B) occurring in carbonate, clay and brucite endmembers, after baseline subtraction.

Table 4
Numerical relationship between 4.6 µm band parameters and GPR18-carbonate wt% content in the mixtures.

Feature wavelength:	X = carbonate GPR18 wt%
λ = 4.6 µm	depth = 0.004*X − 0.028
	area = 0.0006*X − 0.007

Carbonate–clay mixtures (with the addiction of forsterite) were also studied by Bishop et al. (2013). They showed that the addiction of carbonate (magnesite) to mixtures resulted in non-linear increasing of band depths with increasing abundance of magnesite. This is consistent with our results, for what concerns the 3.9 µm band. In fact, as we have seen above, the depth and area of 3.9 µm feature in clay endmember are approximately 60% and 40% of depth and area of carbonate endmember, although the clay MLA4 contains only about 10% of calcite. Nevertheless in our study a linear behavior is observed for the 4.6 µm feature (Table 4).

5. Applications to Ceres

These results can be useful in view of the interpretation of new data on Ceres from DAWN spacecraft. Ground-based spectra of Ceres have been interpreted by invoking the presence of brucite, in mixtures with carbonates and clay minerals, phyllosilicates, especially with the aim of justifying the presence of the 3.05 µm absorption feature (Milliken and Rivkin, Nature Geoscience, 2009). In Fig. 17, we plot a comparison between Ceres (adapted from De Sanctis et al., 2015) and the different end-members used in this work. A mixture of clay, brucite and carbonate is also reported. Ceres spectrum shows clearly the carbonate band at 3.9 µm, the OH band at 2.72 µm and the band at 3.05 µm. A broad band is also present between 3.2–3.6 µm. However, Ceres spectrum lacks of absorptions bands between 1 and 2.7 µm.

Our results indicate that the presence of brucite, in mixtures containing carbonates and clay minerals, is essentially revealed by diagnostic absorption features at 0.95 µm, ~2.45 µm and 3.05 µm (Fig. 17). While the 0.95 and 3.05 µm bands are weak and rapidly disappear in mixtures with a brucite content less than 50–70 wt% (depending on carbonate content), the 2.45 µm band is clearly discernible for a minimum brucite content of 10 wt% in mixtures. Thus this 2.45 µm band is the best indicator to reveal the presence of brucite in the mixtures. However, this band was not observed on Ceres surface (Fig. 17), neither from ground based observations (Vernazza et al., 2005; Rivkin et al., 2006) nor from space (De Sanctis et al., 2015; Ammannito et al., 2016). The ~2.45 µm band of brucite is absent from Ceres spectra while we demon-
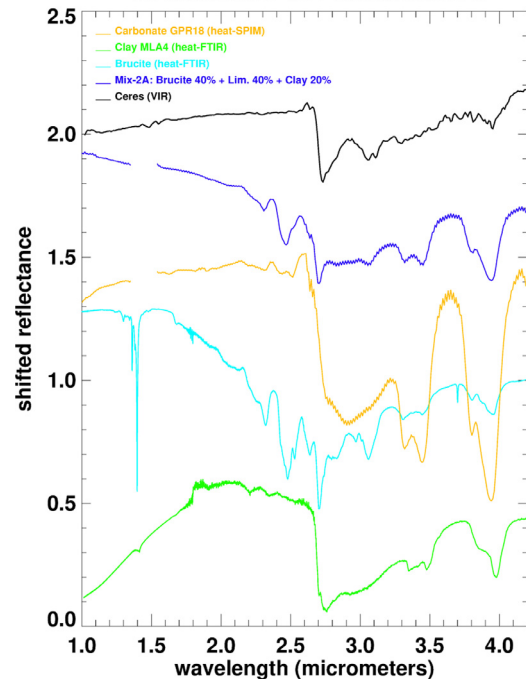

Fig. 17. Comparison between average spectrum of Ceres (Dawn-VIR, from De Sanctis et al., 2015) and endmembers. The spectrum has is also compared with a selected mixture, MIX-2A. The endmembers clay-MLA4 and brucite have been heated for 2.5 h at 250 °C, and then measured with FTIR, in order to reduce adsorbed water. The carbonate-GPR18 has been heated for 4.5 h at 150 °C and then measured with SPIM.

strated that it is discernible in mixtures with clays and carbonates, given its expected band depth, also in mixtures with small amounts of brucite.

Thus, large quantity of brucite on Ceres at global scale is not supported by the telescopic observations neither by Dawn observation with the Visual and Near Infrared Mapping Spectrometer (De Sanctis et al., 2011). VIR observed Ceres surface and the reported average Ceres spectrum (De Sanctis et al., 2015) lacks of absorption features at 0.95 and ~2.45 µm indicating that brucite is absent at global scale. Searching for these bands in the spectral data at higher resolution could be a good method for eventually reveal the presence of brucite in small amount and localized areas at Ceres surface.

6. Conclusions

Four sets of mineral mixtures have been analyzed by means of visible and infrared reflectance spectroscopy in the wavelength range 0.2–5.1 μm. Three endmembers have been used: (i) limestone, GPR18; (ii) clay, MLA4; (iii) brucite, in order to prepare four different ensembles of mixtures. The first three sets are three-component mixtures, characterized by carbonate (GPR18) content equal to 10 wt%, 40 wt% and 70 wt%, and with variable relative proportions of clay and brucite. The fourth set consists of two-component mixtures, containing no limestone.

The analysis of spectral parameters, such as depth and area, of absorption bands both in endmembers and mixtures spectra, allowed to identify several features and trends, and to determine minimum thresholds of detectability of the components in the mixtures.

Brucite is recognizable by its narrow OH-absorption feature at 0.95 μm, with a minimum 50 wt% content in mixtures containing 10 wt% of carbonate (GPR18), or with a minimum 60 wt% content in mixtures containing 40 wt% of carbonate (GPR18). In mixtures containing 70 wt% of carbonate, this brucite feature is no longer discernible. Finally in two-component brucite–clay mixtures, the brucite phase is recognizable for a minimum content of at least 70 wt%.

In the analyzed mixtures, a high content of brucite is also characterized by very steep blue slope in the 1–2.5 μm spectral range. The absorption band at 3.05 μm is clearly visible in mixtures containing at least 70 wt% of brucite; for smaller amounts of brucite, the presence of this feature results in a weak distortion of the 3.0 μm water band. Conversely the strong brucite band at 2.45 μm is present even in mixture with much smaller amount of brucite (10–20%) and is a good indicator of this mineral in the spectra.

The narrow feature at 2.7 μm in brucite is visible in mixtures with low clay content (<20 wt%) and a brucite amount of 60–70 wt% minimum. Where no clay is present, this band is discernible for lower contents of brucite (30 wt% brucite + 70 wt% carbonate).

The clay component (MLA4) in each mixture set is identified by the absorptions near 1.9, 2.2 and 2.4 μm. These features slightly weaken and disappear, as the brucite content increases, while at the same time features at 2.1, 2.3 and 2.45–2.47 μm appear. Clay weak absorption features are discernible for a minimum content of 60–80 wt% (mixtures containing 10 wt% of carbonate), or 60 wt% (mixtures containing 40 wt% of carbonate). In the mixtures containing 70 wt% of carbonate, the 2.2 μm feature (indicative of Al–OH) is no longer visible for a clay content of 30 wt%, that is an upper limit.

Finally the carbonate (GPR18) component is identified by the very strong absorptions near 3.4 and 3.9 μm. These features are also present, although much weaker, in the clay component (due to small amount of carbonate in the sample), and so the bands strengths are slightly influenced by the presence of clay. Nevertheless, the feature at 4.6 μm occurring in the carbonate GPR18 phase is about a factor 10 stronger than in the clay phase, and so is diagnostic of the GPR18 component. The band area at 4.6 μm is 0.007, in the mixtures containing 10 wt% of GPR18, while it is about 0.06 in the GPR18 endmember, thus they are in the ratio 1:10.

By comparing these mixtures spectra with Ceres average spectrum, large quantity of brucite on Ceres surface at global scale is clearly ruled out. The reported average Ceres spectrum (De Sanctis et al., 2015) lacks of absorption features at 0.95, 2.1–2.3 and ~2.45 μm indicating that brucite is absent at global scale. Searching for these bands in the spectral data at higher resolution could be a good method for eventually reveal the presence of brucite in small amount and localized areas at Ceres surface.

Supplementary materials

Supplementary material associated with this article can be found, in the online version, at doi:10.1016/j.icarus.2016.07.002.

References

Ammannito, E., et al., 2016. Distribution of phyllosilicates on the surface of Ceres. Science (in press).

Bishop, J.L., et al., 2013. Coordinated spectral and XRD analyses of magnesite-nontronite-forsterite mixtures and implications for carbonates on Mars. J. Geophys. Res. 118, 635–650. doi:10.1002/jgre.20066.

Carry, B., et al., 2008. Near-infrared mapping and physical properties of the dwarf-planet Ceres. Astron. Astrophys. 478, 235–244. doi:10.1051/0004-6361:20078166.

Clark, R.N., Roush, T.L., 1984. Reflectance spectroscopy: Quantitative analysis techniques for remote sensing applications. J. Geophys. Res. 89 (B7), 6329–6340.

Clark, R.N., et al., 1990. High spectral resolution reflectance spectroscopy of minerals. J. Geophys. Res. 95 (B8), 12653–12680.

Coradini, A., et al., Laboratory Measurements in Support of the DAWN Mission: The SPectral IMaging (SPIM) Facility, EPSC Abstracts Vol. 6, EPSC-DPS2011-1043, EPSC-DPS Joint Meeting 2011.

D'Amico, C., Innocenti, F., Sassi, F.P., Magmatismo e Metamorfismo, cap.2, Le Rocce Magmatiche, UTET, 2nd Edition, 536 p., ISBN-13: 9788802040820, 1989.

De Angelis, S., et al., 2015. The spectral imaging facility: Setup characterization. Rev. Sci. Instrum. 86, 093101-1-15. doi:10.1063/1.4929433.

De Sanctis, M.C., et al., 2011. The VIR spectrometer. Space Sci. Rev. 163, 329–369. doi:10.1007/s11214-010-9668-5.

De Sanctis, M.C., et al., 2015. Ammoniated phyllosilicates with a likely outer Solar System origin on (1) Ceres. Nat. Lett. 528, 241–244.

Fairen, A.G., et al., 2010. Noachian and more recent phyllosilicates in impact craters on Mars. Proc. Natl. Acad. Sci. 107 (27), 12095–12100.

Ehlmann, B.L., et al., 2008. Orbital identification of carbonate-bearing rocks on Mars. Science 322, 1828–1832.

Ehlmann, B.L., Edwards, C.S., 2014. Mineralogy of the martian surface. Annu. Rev. Earth Planet. Sci. 42, 291–315.

Endress, M., Bischoff, A., 1996. Carbonates in CI chondrites: Clues to parent body evolution. Geochim. Cosmochim. Acta 60 (3), 489–507.

Fredriksson, K., Kerridge, J.F., 1988. Carbonates and sulfates in CI chondrites: Formation by aqueous activity on the parent body. Meteoritics 23, 35–44.

Frost, B.R., Beard, J.S., 2007. On silica activity and serpentinization. J. Petrol. 48 (n.7), 1351–1368.

Frost, R.L., Kloprogge, J.T., 1999. Infrared emission spectroscopic study of brucite. Spectrochim. Acta Part A 55, 2195–2205.

Garenne, A., et al., 2013. Gas–solid carbonation as a possible source of carbonates in cold planetary environments. Planet. Space Sci. 76, 28–41.

Johnson, C.A., Prinz, M., 1992. Carbonate compositions in CM and CI chondrites, and implications for aqueous alteration. Geochim. Cosmochim. Acta 57, 2843–2852.

Jones, B.F., Deocampo, D.M., 2003. Geochemistry of Saline Lakes, cap.5.13. In: Holland, Heinrich, Turekian, Karl (Eds.), Treatise on Geochemistry Editors-in-Chief. Published by Elsevier, ISBN: 978-0-08-043751-4 doi:10.1016/B978-0-08-095975-7.09816-8.

King, T.V.V., et al., 1992. Evidence for ammonium-bearing minerals on Ceres. Science 255, 1551–1553.

Lebofsky, L.A., et al., 1981. The 1.7- to 4.2 μm spectrum of Asteroid 1 Ceres: Evidence for structural water in clay minerals. Icarus 48, 453–459.

Michalski, J.R., Niles, P.B., 2010. Deep crustal carbonate rocks exposed by meteor impact on Mars. Nat. Geosci. 3, 751–755.

Mililken, R.E., Rivkin, A.S., 2009. Spectral evidence for a brucite-carbonate alteration assemblage on Ceres. In: Proceedings of the 40th Lunar and Planetary Science Conference, 1481 abstract.

Mililken, R.E., Rivkin, A.S., 2009. Brucite and carbonate assemblages from altered olivine-rich materials on Ceres. Nat. Geosci. 2, 258–261. doi:10.1038/ngeo478.

Morse, J.W., 2003. Formation and diagenesis of carbonate sediments, cap.7.03. In: Holland, Heinrich, Turekian, Karl (Eds.). Treatise on Geochemistry Editors-in-Chief. Published by Elsevier, ISBN: 978-0-08-095975-7.09816-8. doi:10.1016/B978-0-08-095975-7.09816-8.

Murchie, S.L., et al., 2009. A synthesis of martian aqueous mineralogy after 1 Mars year of observations from the Mars reconnaissance orbiter. J. Geophys. Res. 114, E00D06. doi:10.1029/2009JE003342.

Mustard, J.F., et al., 2008. Hydrated silicate minerals on Mars observed by the Mars reconnaissance orbiter CRISM instrument. Nat. Lett. 305–309. doi:10.1038/nature07097.

O'Connor, W.K., et al., 2005. Aqueous Mineral Carbonation. Mineral Availability, Pretreatment, Reaction Parametrics, and Process Studies, Final Report, DOE/ARC-TR-04-002, Office of Process Development, National Energy Technology Laboratory (formerly Albany Research Center), Office of Fossil Energy, US DOE.

Rivkin, A.S., et al., 2006. The surface composition of Ceres: Discovery of carbonates and iron-rich clays. Icarus 185, 563–567.

Russell, C.T., et al., 2004. Dawn: A journey in space and time. Planet. Space Sci. 52, 465–489.

Staudigel, H., 2003. Hydrothermal alteration processes in the oceanic crust, cap.3.15. In: Holland, Heinrich, Turekian, Karl (Eds.). Treatise on Geochemistry Editors-in-Chief. Published by Elsevier, ISBN: 978-0-08-043751-4 doi:10.1016/B978-0-08-095975-7.09816-8.

Tonui, E., et al., 2014. Petrographic, chemical and spectroscopic evidence for thermal metamorphism in carbonaceous chondrites I: CI and CM chondrites. Geochim. Cosmochim. Acta 126, 284–306.

Toppani, A., et al., 2005. A 'dry' condensation origin for circumstellar Carbonates. Nat. Lett. 437, 1121–1124. doi:10.1038/nature04128.

Vaniman, D.T., et al., 2014. Mineralogy of a Mudstone at Yellowknife Bay, Gale Crater, Mars. Science 343. doi:10.1126/science.1243480.

Vernazza, P., et al., 2005. Analysis of near-IR spectra of 1 Ceres and 4 Vesta, targets of the Dawn mission. Astron. Astrophys. 436, 1113–1121.

Zolotov, M.Y., 2009. On the composition and differentiation of Ceres. Icarus 204, 183–193. doi:10.1016/j.icarus.2009.06.011.